Advances in Aircraft and Spacecraft Science, *Vol. 1, No. 4 (2014) 409-425*
DOI: http://dx.doi.org/10.12989/aas.2014.1.4.409

Valve actuation effects on discrete monopropellant slug delivery in a micro-scale fuel injection system

M. Ryan McDevitt[a] and Darren L. Hitt[*]

Mechanical Engineering Program, School of Engineering, University of Vermont, Burlington, VT 05405, USA

(Received February 13, 2014, Revised March 13, 2014, Accepted May 16, 2014)

Abstract. Converging flows of a gas and a liquid at a microchannel cross junction, under proper conditions, can result in the formation of periodic, dispersed microslugs. This microslug formation phenomenon has been proposed as the basis for a fuel injection system in a novel, 'discrete' monopropellant microthruster designed for use in next-generation miniaturized satellites. Previous experimental studies demonstrated the ability to generate fuel slugs with characteristics commensurate with the intended application during steady-state operation. In this work, numerical and experimental techniques are used to study the effect of valve actuation on slug characteristics, and the results are used to compare with equivalent steady-state slugs. Computational simulations of a valve with a 1 ms valve-actuation cycle show that as the ratio of the response time of the valve to the fully open time is increased, transient effects can increase slug length by up to 17%. The simulations also demonstrate that the effect of the valve is largely independent of surface tension coefficient, which is the thermophysical parameter most responsible for slug formation characteristics. Flow visualization experiments performed using a miniature valve with a 20 ms response time showed less than a 1% change in the length of slugs formed during the actuation cycle. The results of this study indicate that impulse bit and thrust calculations can discount transient effects for slower valves, but as valve technology improves transient effects may become more significant.

Keywords: microfluidics; micropropulsion; CFD

1. Introduction

A recent focus of the aerospace industry has been in the development of microthrusters for satellites in the 1.0 to 10.0 kg range, often known as "nanosats". Nanosats are of interest for NASA and the DoD because of their ability to reduce satellite life-cycle costs while performing valuable scientific and defense missions. A survey of past and current missions involving nanosats, which can be found in Bouwmeester and Guo (2010), indicates that the capabilities of nanosatellites are technologically limited on several fronts including power, communication and thruster subsystems. The thrusters, which are the propulsion system tasked with positioning and orbital maintenance, are a particular challenge because of the low levels of thrust, on the order of

∗Corresponding author, Ph.D., E-mail: darren.hitt@uvm.edu
[a]Ph.D. Student, E-mail: ryan.mcdevitt@uvm.edu

http://www.techno-press.org/?journal=aas&subpage=7 ISSN: 2287-528X (Print), 2287-5271 (Online)

Table 1 GSFC operating requirements as presented in Hitt *et al.* (2001)

Propulsion system parameter	Target value or range
Thrust level	500 μN
Impulse bit	1-100 μNs
Specific impulse	160 s
Mass	< 0.1 kg

micronewtons, required to make precise changes in position that may be required as part of a mission. Micropropulsion is an area of ongoing research with many candidate systems proposed, including electric propulsion systems and liquid and solid chemical propellant systems. Reviews of micropropulsion strategies for nanosat microthrusters can be found in Janson (2008).

Monopropellant-based propulsion is an attractive scheme for microthruster applications since it offers a combination of relatively high energy density and simplicity of design. The latter is especially significant for the construction of miniaturized propulsion systems. The first prototype monopropellant microthruster reported in the aerospace literature was based on hydrogen peroxide and developed using MicroElectroMechanical Systems (MEMS) techniques at NASA/Goddard Space Flight Center (Hitt *et al.* 2001). As part of that study, the operating characteristics required for the thruster subsystem were presented, and are shown in Table 1.

The typical operation of a microthruster consists of the delivery of a specified amount of impulse to the spacecraft and is thus inherently transient in nature. For a monopropellant microthruster (indeed, any liquid chemical microthruster) this involves the throttling of the propellant via a microvalve. During the shutdown process there will be an unavoidable residual thrust resulting from the finite actuation of the valve and, for micropropulsion applications, the impact of the associated residual thrust and impulse may be significant. For example, it has been determined from numerical simulations of microthruster nozzles, based on the geometry of the NASA/GSFC prototype that the residual thrust produced during the shutdown of the thruster may lead to a residual impulse which is more than twice the design impulse bit (Kujawa and Hitt 2005, Louisos and Hitt 2011). Given the potentially troublesome throttling issues associated with MEMS-based microthruster designs, it would be highly desirable to have an alternative method capable of producing ‘discrete’ impulses for attitude control and adjustment. Indeed, such a scheme already exists for solid propellants in the DARPA ‘digital microthruster’ (Lewis *et al.* 2000).

One possible strategy is to use a system, shown in Figure 1, to deliver the monopropellant to the thruster in discrete quantities (‘slugs’) to produce the ‘digital propulsion’ effect (McCabe *et al.* 2012). In this process, the liquid monopropellant and a second immiscible inert gas converge at a microscopic cross junction. The array of monopropellant slugs formed will flow through the outlet channel where they undergo a chemical decomposition in an in situ catalyst bed. This will be embedded directly into the channel thereby simplifying the geometry as well as decreasing the footprint on the chip. The inert fluid will pass through the bed chemically unaffected. The decomposition products then flow directly into a supersonic nozzle to convert the thermal energy into kinetic energy. By making the impulse bits sufficiently small, a target impulse can be delivered with the passage of a set number of slugs, which effectively increases the resolution of the valve timing. While conceptually straightforward, the actual operation will depend principally upon the characteristics of the monopropellant slugs, which are formed.

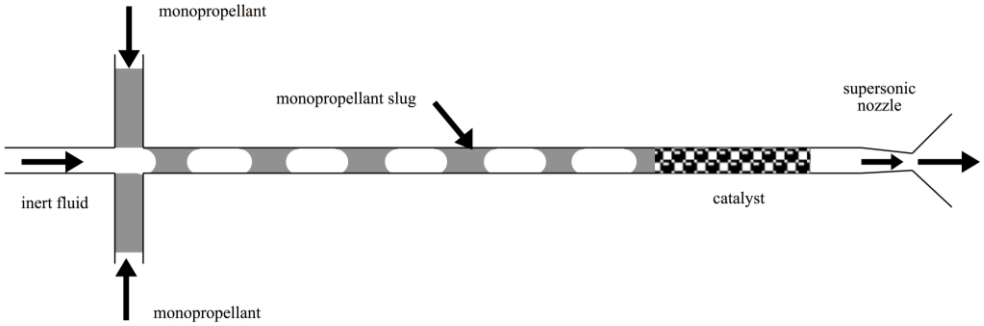

Fig. 1 A schematic diagram depicting the envisioned operation of the discrete mono- propellant thruster. Flows of a monopropellant and a gaseous inert fluid converge at a 90° junction. The result is a periodic sequence of discrete monopropellant slugs, which propagate down the channel where they are chemically decomposed in a catalytic bed. The energetic gases of decomposition in combination with the inert gas are then expanded in a converging/diverging supersonic nozzle to produce the target impulse for that slug

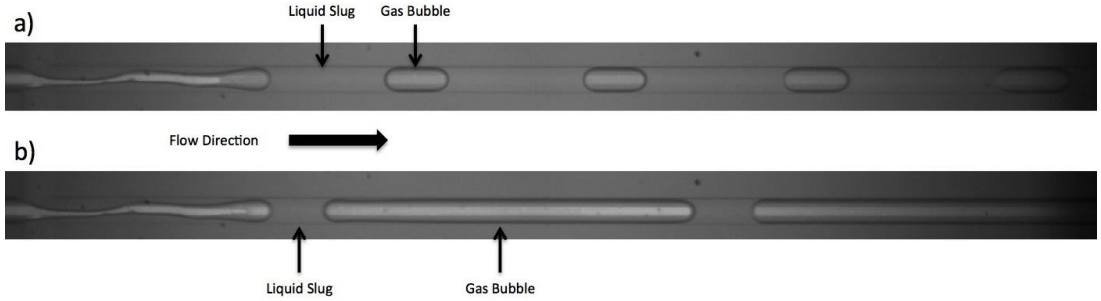

Fig. 2 Images of slug formation in a 50 μm microchannel. The inlet pressures in (a) are all set at 30 psi. In 9b) the liquid inlet pressure is set at 30 psi and the air inlet pressure is set at 30.6 psi resulting in very different slug characteristics

Recent studies in the microfluidics literature have demonstrated that two immiscible liquids at a microscopic *T*-junction can be used to create slug structures that are periodic and highly repeatable (Thorsen *et al.* 2001, Garstecki *et al.* 2006). While these studies provide a foundation for further research they are limited in practical application due to the need to carry a second pressurized liquid on the satellite. The efficiency of the catalytic process in generating thermal energy may also be decreased due to the need to heat the inert liquid. In addition, if the secondary liquid is an oil, fouling will occur in the catalyst bed. Previous work has been performed by Cubaud and Ho (2004), and Cubaud *et al.* (2005) for gas-liquid flows in larger microchannels O[100μm]. These microchannels generate slugs that are too massive for the intended microthruster application, and since the effects of surface tension will increase with decreasing channel size, smaller channels may exhibit different behaviors. In McCabe *et al.* (2012), a pressure-driven system that was an order of magnitude smaller than that studied by Cubaud and Ho (2004), was created to characterize the microslug formation by the inlet pressure ratio. They found that controlling the pressure ratio at the inlets allowed them to create steady, periodic microslugs of different sizes and lengths. An example of the variability of the slug characteristics is shown in Fig. 2.

In their experimental study, McCabe *et al.* (2012) were able to demonstrate a reduction in fuel delivery of nearly 50% for a given time period using this process, which would allow the monopropellant microthruster to meet the design criteria using currently available microvalve technology. While this finding was an important demonstration of the feasibility of the discrete, monopropellant microthruster concept, the testing methodology in that experiment required that the microfluidic system be allowed to stabilize by running the system for several minutes before collecting data. This procedure attempts to eliminate sources of experimental error that can occur in a microfluidic system, such as air bubbles in the line, but it also serves to remove the effects of valve actuation from the data collected. As the proposed MEMS-based thruster will primarily operate in this transient region, these effects could potentially alter the slug characteristics compared to the steady-state slug characteristics that are typically reported in the literature. Potential alterations could include post-actuation inertial effects, lag in the slug formation process during valve opening or changes in the hydrodynamic resistance of the system due to the presence of the microvalves. Any of these effects could dramatically affect the slug characteristics compared to the steady state, and thus the impulse bit and thrust.

In this study, numerical and experimental techniques, first presented in McDevitt and Hitt (2011) and McCabe *et al.* (2011) respectively, were used to determine the slug characteristics and formation process of the microthruster during the actuation of the valves controlling the inert gas and the monopropellant. The numerical simulations were used to characterize the sensitivity of the slug formation process to changes in the valve-actuation profile and surface tension coefficient during a valve-actuation cycle. These results are then used to calculate the valve actuation effects on the minimum impulse bit and effective thrust of an idealized microthruster. To complement the simulations, flow visualization experiments were performed to provide a qualitative comparison with the numerical results.

2. Computational methods

To study the effects of transient operation, both computational and experimental techniques were used. The numerical studies used a quasi-3D model of a microchannel cross-junction and used the level set method to track the interface between the two phases. This computational model allowed for the interrogation of flow characteristics that would be difficult or impossible to study experimentally. The experiments consisted of flow visualizations using a pressure-driven microfluidic flow system that has been designed to deliver gas and liquid phases from upstream pressurized reservoirs to a cross junction.

For the experiments, H_2O has been used in lieu of actual H_2O_2 since its properties are similar and we do not wish to incur any reaction at this stage of the work. Air was used instead of a chemically inert gas such as Ar or N_2. The predominant flow properties in microfluidic flow analysis are surface tension and viscosity. As the two fluid substitutions are similar in these parameters to their analogues, they should not present any significant differences in the behavior observed.

2.1 Computational model and numerical algorithm

2.1.1 Computational geometry

A quasi-3D model of the microchannel used in the flow visualization experiments was built for

Fig. 3 The computational domain used for the simulations

the simulations. The experimental geometry had a 50 μm by 20 μm cross sectional area, and had inlet channel lengths of 3 mm and an outlet channel length of 80 mm. To simplify the geometry and reduce computational overhead, the computational domain was reduced to an air inlet that is 450 μm (9 channel widths) long, 2 fuel inlets which are 150 μm (3 channel widths) long and an outlet channel which is 2250 μm (45 channel widths) long. The resulting computational domain is shown in Fig. 3.

2.1.3 Governing equations

The flow field is governed by the incompressible Navier-Stokes equations

$$\nabla \cdot \mathbf{u_i} = 0 \tag{1}$$

$$\rho_i \frac{\partial \mathbf{u_i}}{\partial t} + \rho_i(\mathbf{u_i} \cdot \nabla)\mathbf{u_i} = \nabla \cdot \left[-\mathbf{pI} + \mu_i\left(\nabla \mathbf{u_i} + \nabla \mathbf{u_i^T}\right)\right] + \vec{\mathrm{F}}_{\mathrm{ST}} \tag{2}$$

where **u** is the velocity of the fluid, ρ is the fluid density, p is the pressure, μ is the dynamic viscosity, $\mathrm{F_{ST}}$ is the surface tension and the subscript i corresponds to the appropriate phase. To track the interface between the two different fluids, the level set method was used. In the level set method, the discontinuity between the two discrete phases is represented with the level set function ϕ, a continuous function bounded by zero and unity that represents the distance from the interface at all points in the domain (Sethian 1998). The ϕ=.5 isocontour then represents the interface between the two phases. As the flow field is calculated, the movement of the interface is calculated

$$\frac{\partial \phi}{\partial t} + \mathbf{u} \cdot \nabla \phi = \phi(1-\phi)\frac{\nabla \phi}{|\nabla \phi|} \tag{3}$$

The discontinuity in density (ρ) and viscosity (ν) are smoothed across the interface using Eqs. (4) and (5)

$$\rho = \rho_1 + (\rho_2 - \rho_1)\phi \tag{4}$$

$$\upsilon = \upsilon_1 + (\upsilon_2 - \upsilon_1)\phi \tag{5}$$

where ρ_1 and ν_1 are the density and kinematic viscosity of the first fluid, and ρ_2 and ν_2 are of the second fluid. The surface tension term, in Eq. (2), at a point $\vec{x}$ can be calculated from:

$$\vec{F}_{ST}(\vec{x}) = \sigma\kappa(\vec{x})\hat{n}(\vec{x}) \tag{6}$$

where σ is the surface tension coefficient, $\hat{n}$ and κ are the unit normal and curvature of the interface, respectively. In the level set method, $\hat{n}$ and κ can be calculated from ϕ using

$$\hat{n} = \frac{\nabla \phi}{|\nabla \phi|} \tag{7}$$

$$\kappa = -\nabla \cdot (\frac{\nabla \phi}{|\nabla \phi|}) \tag{8}$$

The surface tension equation can then be recast in terms of the surface tension coefficient and the level set function

$$\vec{\mathrm{F}}_{\mathrm{ST}}(\vec{x}) = \sigma(-\nabla \cdot \frac{\nabla \phi}{|\nabla \phi|})\nabla \phi \tag{9}$$

In this formulation, the surface tension represents a volume force that is spread across the width of the interface. This new force is only equal to the surface tension in the limit as the thickness of the interface goes to zero, which places an upper bound on the maximum width of the interface. If the interface gets too small, however, the discontinuity in density and viscosity cannot be properly smoothed, which yields difficulties in computing the solution. The surface tension can be varied by changing the surface tension coefficient (σ).

These governing equations were solved in COMSOL 4.2a, an FEA-based multiphysics solver. The COMSOL implementation uses a modified version of the level set, designed to improve the mass conservation, developed by Olsson *et al.* (2005). In this method the movement of the level set function (ϕ) is corrected by using a modified advection equation

$$\frac{\partial \phi}{\partial t} + \mathbf{u} \cdot \nabla \phi = \gamma \nabla \cdot (\epsilon \nabla \phi - \phi(1-\phi)\frac{\nabla \phi}{|\nabla \phi|} \tag{10}$$

where γ represents a reinitialization parameter that predicts where the interface has moved to since the last time step and ε represents an estimated interface thickness. For numerical stability, the minimum mesh size should be O[ε] and γ should be roughly equivalent to the maximum velocity of the flow.

Due to the intense computational demands of simulating the flow in 3D, using a 2D simulation was desirable for parametric studies. In Qian and Lawal (2008), a strong connection between the 2D and 3D simulations of microslug generation in microchannels was found. To verify that a similar connection exists in this study, a 3D model of the junction was simulated and compared against the 2D model. The original models showed a discrepancy, but this was corrected by adding a "shallow channel" term

$$\vec{F}_{\eta} = \frac{12\eta \vec{u}}{h^2} \tag{11}$$

where $\vec{F}_{\eta}$ represents a body force resulting from the channel top and bottom. This quasi-3D flow compares very closely to the full 3D simulation and verifies that a 2D simulation, with this shallow-channel term, is appropriate for simulating the flow.

2.1.3 Boundary conditions

In the motivating experiments by McCabe *et al.* (2011), the microfluidic system is pressure driven and uses a pressure differential at the cross junction to generate the slug patterns. As the actual pressures of the liquid and gas at the junction are unknown, equivalent velocity conditions were selected that most nearly replicated the experimental observations in McCabe *et al.* (2011). To do this, the liquid inlet velocity is fixed at .4 m/s, with an air inlet velocity that ranges between .2 and .4 m/s. These velocities represent the lower and upper bounds of the slug generation process; decreasing the flow rate of the continuous phase further results in the dispersed phase

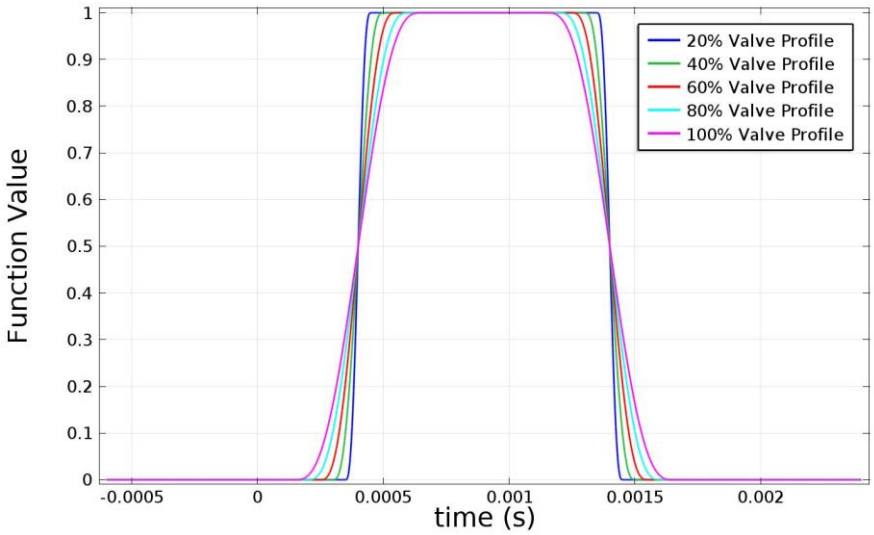

Fig. 4 Plot of the valve profiles simulated

completely filling the channel, while increasing the continuous phase flow rate prevents the dispersed phase from entering the channel.

To model the effects of actuation on the slug formation process, a series of valve-actuation profiles, modeled as smoothed rectangle functions between 0 and 1 and shown in Fig. 4, are applied equally to the gas and liquid inlets. The valve-actuation profile can be characterized by the total duration of a single actuation cycle and the ratio of the response time to the fully open time of the valve. For these simulations, the nominal actuation cycle is 1 ms, with the ratio of response time to fully open time ranging between 20% and 100%. The studies of surface tension coefficient used a fixed valve profile, with a 1 ms actuation time and were limited to a singe response ratio of 20%.

For the implementation of the level set within COMSOL, a wetted wall boundary condition is used. This boundary condition uses a fixed contact angle (θ) and a slip length (β) that is defined as the distance perpendicular to the wall at which the velocity can be extrapolated to zero.

2.1.4 Grid generation and convergence

To accurately model multiphase flow, the grid must be smaller than the projected interface thickness at all locations that it may travel. To increase solution speed, adaptive mesh refinement was used. This method generates a coarse unstructured mesh within the computational domain. The number of elements is then increased in regions where there is a gradient of the level set function (i.e., at the interface between the two fluids). Convergence is achieved when the interface is resolved, as determined by the percent difference change in interface thickness. At successive time steps, this process is repeated to ensure that the mesh adapts to the changing topology of the interface. While this method precludes traditional grid convergence studies, the continuous refinement of the mesh is intended to keep it optimized.

To confirm that the results generated while using adaptive mesh refinement are comparable to a fixed mesh simulation, models were solved using each method. While there are qualitative differences between the two simulations, it is worth noting that the primary goal of this work is to

characterize the performance of the fuel injection system, which is necessarily going to involve the measurement of many slugs. Thus small variations in individual slugs are going to be less important than the average slug characteristics. For the model studied, the slugs in the model with adaptive mesh refinement were 2% larger than on a fixed mesh. As the processing time for a single simulation was an order of magnitude smaller (2 hours for adaptive mesh refinement vs. 20 hours for fixed mesh) and this study would involve a number of simulations, adaptive mesh refinement was deemed to be acceptable.

2.2 Slug analysis and thrust calculations

To determine thrust level and impulse bit, both the pinch-off frequency and the microslug length were measured. Using a method developed by McCabe *et al.* (2011) for analyzing images generated during flow visualization experiments, contour plots of the volume fraction of the liquid phase in the computer simulations were output as images to MATLAB where intensity data along the centerline of the channel was extracted. Slug length was calculated directly from the images by locating the position of the gas/liquid interfaces bounding an individual slug. The formation frequency is calculated from the total number of slugs divided by the simulation time.

From the knowledge of the slug size and the formation frequency, an effective time averaged mass flow rate may be computed. Assuming complete chemical decomposition of the hydrogen peroxide monopropellant in the catalytic chamber and 100% efficiency in the conversation to thrust by the nozzle, an upper bound for the time averaged thrust production can be established

$$F_t = (\rho L_s A_c f) I_{sp} g_0 \tag{12}$$

where L_S is the average slug length, A_C is the cross-sectional area of the channel, f is the slug formation frequency, I_{sp} is the specific impulse of the monopropellant and g_0 is the acceleration due to gravity. The I_{sp} of 90% HTP H_2O_2 is known to be 154s from the rocket propulsion literature. In contrast, cold gas propulsion schemes typically have I_{sp} values on the order of 70s or roughly half that of the H_2O_2. As the mass flow rate of the gas in this system is several magnitudes smaller than the liquid phase, the gas contribution to the thrust can be neglected.

The impulse was calculated by dividing the total thrust by the frequency, which makes it dependent only on slug length. Finally, the impulse during an actuation cycle can be calculated from the impulse delivered during a single valve actuation.

$$I = (\rho L_s A_c) I_{sp} g_0 \tag{13}$$

2.3 Experimental apparatus

The pressure-driven microfluidic flow system uses compressed air and pressurized deionized water. The microfluidic chip, which contains the flow channels, is manufactured offsite by Micralyne Inc. The chip is made of Schott Borofloat glass that allows for straightforward optical analysis. The chip contains four access holes three of which lead to channels that merge into a 90° junction and a fourth serves as the outlet. The chip layout is shown in Fig. 5.

Tubing is connected via Upchurch Scientific NanoPorts mounted to the glass directly above the access holes. This tubing is connected to Kuhnke microvalves that have 20 *ms* actuation time, and are controlled via a function generator sending a 1 Hz pulse with a 100% duty cycle. Compressed

Fig. 5 The geometry of the microchannel used for flow visualization experiments

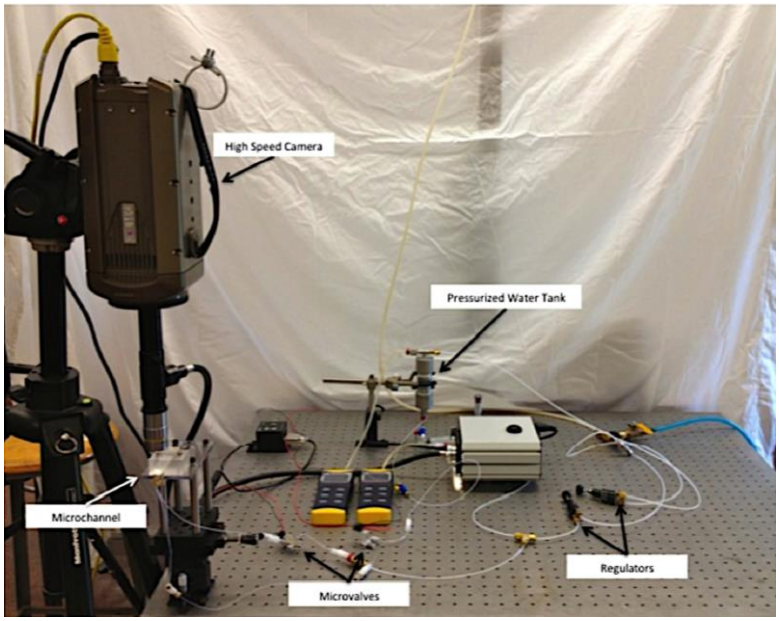

Fig. 6 Photo of the experimental apparatus used for the flow visualization experiments

air supplies the air line as well as the pressure for the water reservoir. Digital manometers are used to obtain pressure readings at the air and water reservoirs. The water pressure in each of the two water lines must be equal at the inlet ports for the system to exhibit the desired flow patterns. This is done by limiting, as much as possible, the pressure drops due to flow resistance before the two inlet ports. The compressed air is initially filtered to 7 μm and each water line is again filtered using 2 μm microfilters to eliminate any clogging in the microchannel which may lead to a pressure drop causing a bias in the system.

The base pressure of the system is set by the water pressure and the air pressure can range from the base pressure (Δp=0 psi) to Δp=0.6 psi below the water pressure. The lower limit of the air pressure corresponds to entirely water in the outlet channel. The upper limit is the point at which the slug formation becomes unstable resulting in a transition from periodic slug formation to a core-annular configuration, the latter being unacceptable for our application.

For these experiments, the system was run with the valves open until the system was stabilized, and producing regular slugs. Once this point is reached, the valves are triggered and cycle based on the specified frequency. Flow visualization is performed using an Infini-Tube In-Line video system equipped with a fiber optic light source and a Phantom V310 High Speed Camera from

Vision Research. Images were captured at 20,000 FPS of 8-bit grayscale at a resolution of 1024× 96 pixels. A photograph of the experimental setup is shown in Fig. 6.

3. Results

The results of this investigation are weighted towards the numerical simulations, as they were used to study the slug formation process during a valve-actuation cycle (1 ms) that would be possible for a MEMS-based microvalve. The effects of changes in valve-actuation profile and surface tension coefficient, both of which are difficult to modify experimentally, were examined. The flow visualization experiments were performed with a miniature solenoid valve, which has a valve-actuation cycle that is an order of magnitude longer (20 ms) than the microvalve that would be used in the envisioned prototype. Due to this difference, the experiments are not performed as an explicit verification of the numerical results; rather they serve as a complementary piece of the study that aims to show qualitative similarities.

3.1 Numerical results

Using the methodology described previously, a series of simulations were performed to investigate the effects of valve-actuation profile and surface tension coefficient on the slug formation process. Fig. 7 shows a time sequence of results for an example simulation. To analyze these results, in each study the first slug produced after the valve is opened (post-actuation slug) is compared to the average slug length during the simulation. This allows for a direct comparison between the slug generated during valve actuation and the slugs that would be generated in a steady-state system at the same inlet conditions and thermophysical properties.

(a) $t = .4ms$

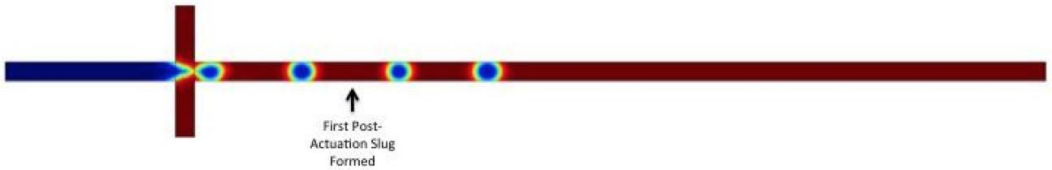

(b) $t = 1.4ms$

Fig. 7 Sample of the results generated during transient operation. The fuel is represented in red, with the air represented in blue. The valve closes at .4 ms and reopens at 1 ms

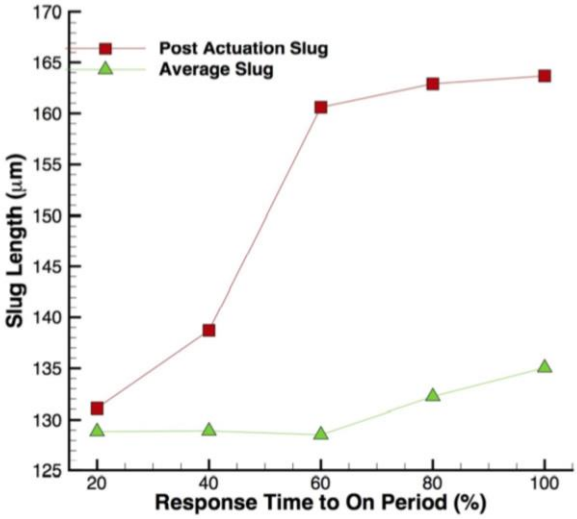

Fig. 8 Comparison of the average slug length with the first slug generated after the valve opening as the ratio of the response time to the on period is increased. As the ratio decreases the slug formation process becomes essentially insensitive to the valve actuation

3.1.1 Effects of valve-actuation profile

The response time of a valve has a direct impact on the mass flow rate through that valve for a single actuation. For a desired valve opening, a slower response time will lead to a longer valve-actuation cycle and an increase in fluid allowed through the valve. To characterize this effect on the slug formation process, the length of a post-actuation slug generated for a series of different valve-actuation profiles was compared to the length of the average slug and the results are plotted in Figure 8. This plot shows that the valve-actuation profile corresponding to the fastest response time has a limited impact (2.2%) on the post actuation slug length compared to the average slug, while increasing the ratio of the response time to the fully open time results in up to a 17% difference in slug length. The largest jump in slug length occurs between the 40% and 60% ratio; this appears to be the threshold where the flow velocity related to the valve actuation is significant enough to impact slug length.

In a steady-state system the characteristics of slugs formed are highly dependent on inlet flow conditions, specifically the baseline flow rate and the flow rate differential. While changes in the valve-actuation profile are applied equally to all three inlets, and thus the flow rate differential remains constant, changes in the response time have the effect of changing the baseline flow rate of the system which has a direct effect on the slug that is formed during this actuation.

One point of interest is that this effect is limited to the first post-actuation slug. Sub- sequent slugs are the same length as the slugs that were formed before the actuation cycle begins, which further demonstrates that the effect of the actuation is due to the impact on the baseline flow rate during startup and shutdown. The consequences of this single slug being larger will be discussed further below.

3.1.2 Effects of surface tension coefficient

A recent study examining steady-state slug formation by McDevitt and Hitt (2011) considered the effects of changes in thermophysical properties on slug characteristics and found that surface

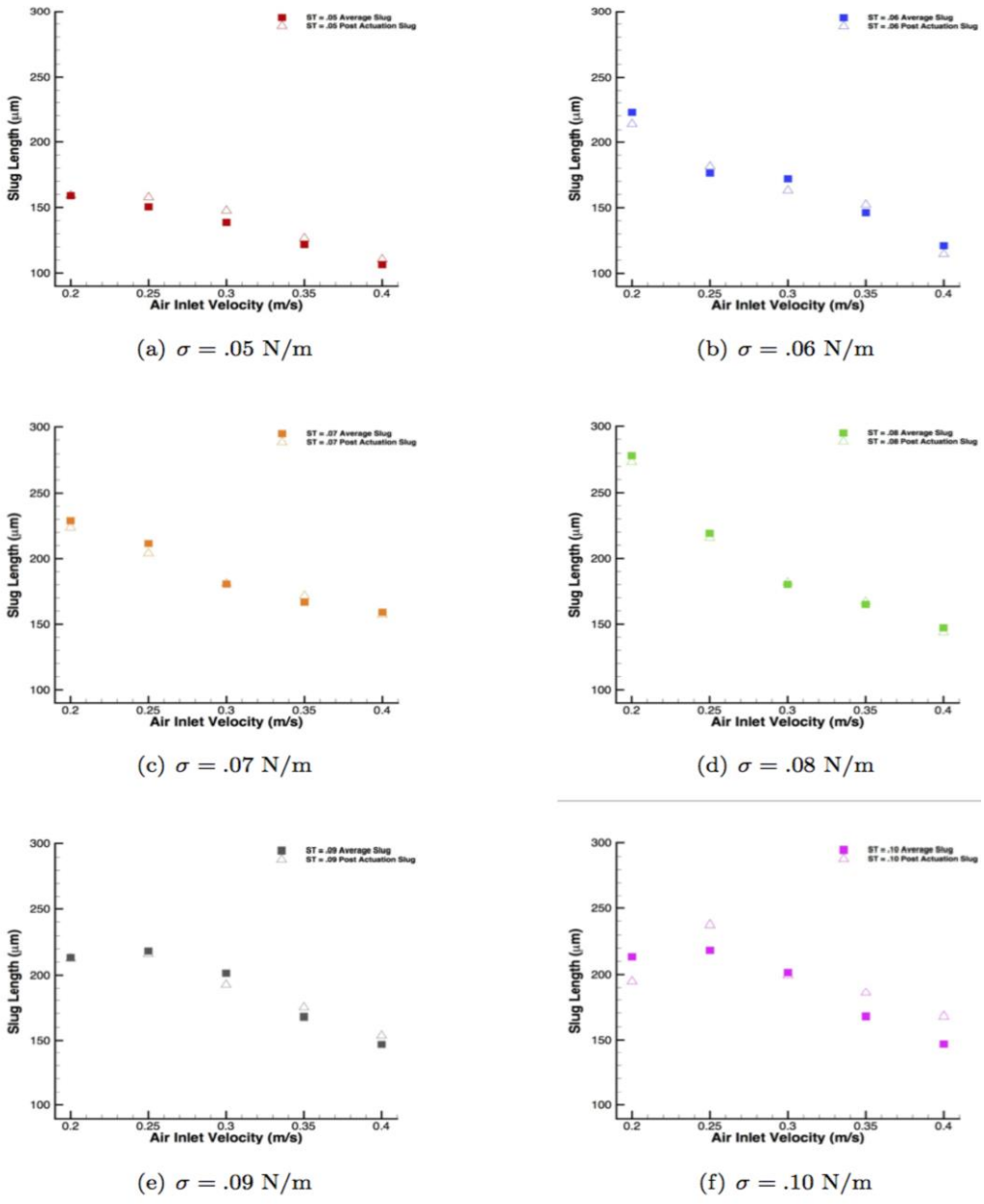

Fig. 9 Plots of average slug and first slug post-actuation at different surface tension coefficients. There is little difference in the slug length measured, and the observed difference does not appear to be correlated to inlet conditions or the surface tension coefficient

tension coefficient was the dominant property in determining slug length. Surface tension can be affected by changes in temperature or due to contamination of the monopropellant, both of which could happen during a space mission. As the valve alters the inherent force balance of the system, surface tension and inertia could be affected, with a consequent effect on slug characteristics.

To study this effect, the surface tension coefficient was varied between .05 N/m and .10 N/m at flow rates between .2 m/s and .4 m/s. Fig. 9 shows the average slug length and the post-actuation slug formed for the different parameters. The average slug length in each case is consistent with the results presented in McDevitt and Hitt (2011); increasing the surface tension coefficient leads to an increase in slug length, with this increase being most pronounced between .06 and .08 N/m. For each surface tension coefficient studied, the length of the post-actuation slug exhibited the same behavior, and in general was very similar to the average slug. For post-actuation slugs that deviate from the average slug, there does not appear to be any trend, indicating these deviations may be related to inaccuracy in determination of the slug length.

3.1.3 Effective thrust and impulse bit

Using the slug lengths from the previous results, the microthruster performance during valve actuation is calculated and compared to the performance of the microthruster during steady-state operation. For the comparison of valve-actuation profile, the metric of interest was the impulse bit. This metric is defined by a single valve opening and closing, so changes in slug length due to the valve-actuation profile will have a large impact on the performance of the thruster. To estimate this effect, the minimum impulse bit of an idealized thruster is calculated from the total slug lengths of all slugs generated during a valve-actuation cycle.

This impulse is compared to an idealized thruster operating at steady state for an equivalent time period. The results of these calculations are plotted in Fig. 10. The impact of the longer post-actuation slug is necessarily diminished by the averaging with the subsequent slugs, with a resulting 12.5% difference between the actuated impulse bit and the impulse of a steady-state system over an equivalent time period. Clearly the overall impact scales with the number of slugs formed during the actuation cycle.

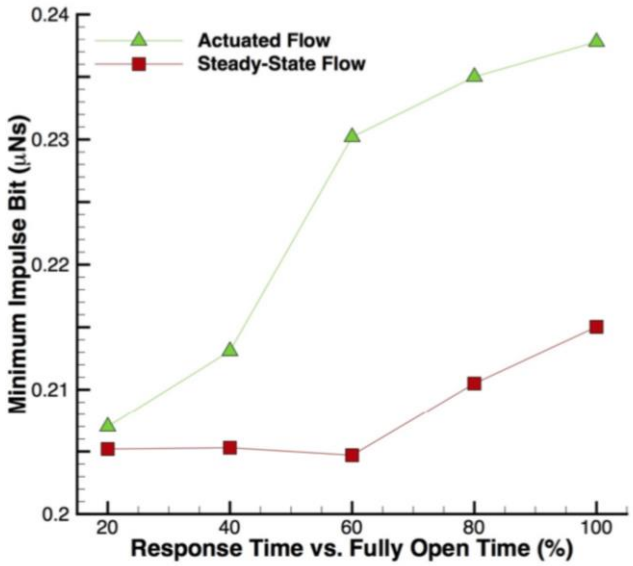

Fig. 10 Plot of the effect of valve actuation on the minimum impulse bit of the thruster as the ratio of response time to on period is increased. As the ratio reaches 100% (i.e., actuating at the limit of the valve) this effect reaches a 3% increase in impulse generated due to the actuation effect

Table 2 Percent difference between actuated and steady-state thrust

	Surface Tension Coefficient (N/m)					
Inlet Velocity (m/s)	.05	.06	.07	.08	.09	.10
.20	0.08	1.91	1.15	0.90	0.21	0.19
.25	2.31	1.37	1.86	0.80	0.52	1.59
.30	3.03	2.73	0.09	0.38	2.28	0.43
.35	1.89	1.98	1.40	0.57	1.95	0.65
.40	1.84	2.77	0.60	1.24	2.19	0.85

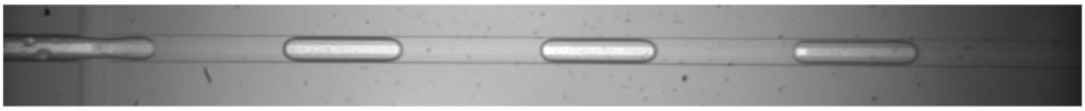

(a) Opening 1

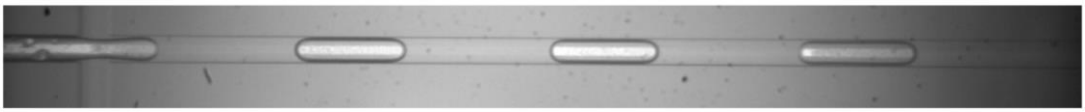

(b) Opening 2

Fig. 11 Sample of the flow visualization images gathered during a series of valve actuations for an inlet pressure differential (Δp) of 0 psi at a baseline pressure of 30 psi

It is worth noting that even with the slowest valve actuation, where the response time is equal to the on period, the minimum impulse bit is .24 μNs, which is well below the target specification. Valve actuation has an impact on minimum impulse bit, but all systems examined are still capable of meeting the design requirements.

In a similar fashion, the impact of surface tension on the thrust and impulse production was calculated and compared to the time averaged thrust for a system assuming no valve actuation. The percent difference in thrust between an actuated firing and an equivalent steady-state system was calculated for each inlet condition and surface tension coefficient and the results are shown in Table 2. As several slugs are formed for a single valve actuation, the non-uniform post-actuation slug has a limited effect on the total thrust produced when compared to the steady-state equivalent. In general, this effect is less than 1% with a maximum difference of 3.03%. As there is no clear correlation with increases in flow rate or surface tension coefficient, the differences can be attributed to lack of resolution in the contour plots used to calculate the length of the slugs.

3.2 Experimental results

A series of flow visualization experiments were performed to provide an empirical comparison to the predictions obtained from the numerical simulations. Using high-speed photography, a sequence of images that spans an entire valve-actuation cycle was captured. Using these images, a comparison can be made between the first slug generated after the valve was opened at separate intervals. Fig. 11 shows a single inlet condition (30 psi and ΔP=0 psi) at two successive valve openings. These images show that the first slug generated after the opening of the valve is similar

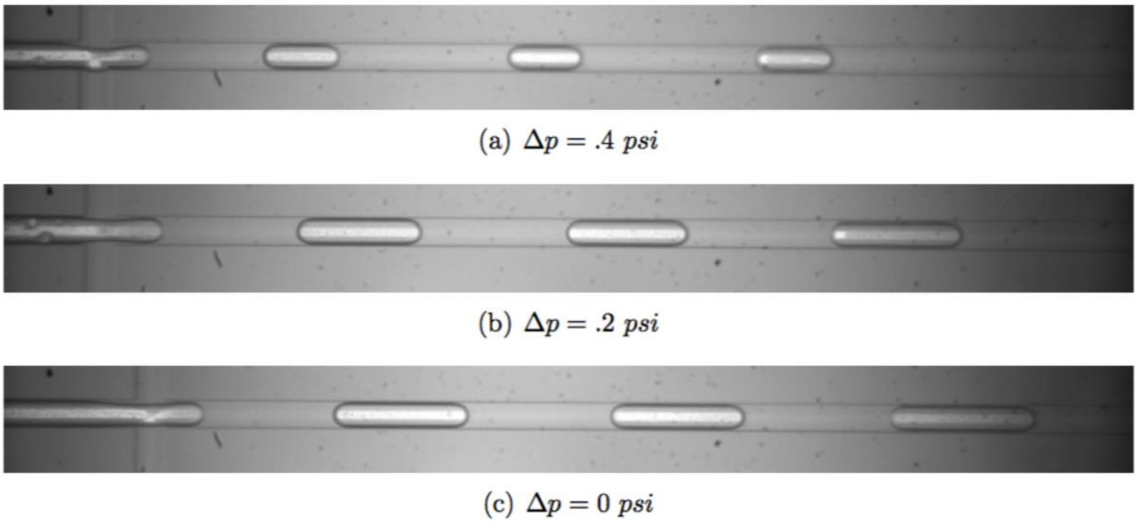

Fig. 12 Comparison of slugs generated during valve opening for a baseline of 30 psi and the gas inlet pressure ranging from .4 to 0 psi below the liquid inlet pressure

to the other slugs generated after the valve opening and that these characteristics recur for subsequent valve openings. Image analysis confirms that the slug length of the post-actuation slug is within 1% of subsequent slugs and that this similitude applies across ensuing valve openings. As the experimental uncertainty when determining the length of the slugs is at a minimum 1.8%, these slugs are equal within the limits of the observations.

Flow visualizations were captured for 3 inlet pressure differentials (Δp=.4, .2 and 0) at a baseline pressure of 30 psi. In all cases, the slugs generated immediately after the valve opening were within 1% of the average slug. A sample of these images is presented in Fig. 12. These results further confirm that the effect of the valve is to temporarily change the inlet baseline pressure, but this effect is limited in its impact, as the valves used are not MEMS-based and have much longer response times.

It is interesting to note that while operating the valves in a continuous on mode, the slug characteristics (length and frequency) were different from previous experimental observations on the same microfluidic channel. This change is most likely attributed to the change in hydrodynamic resistance that the miniature valves present. Identical valves were used for the gas and liquid inlets and the resulting pressure drop across the valve in the liquid line will be greater. This change in pressure has an impact on the pressure differential at the junction (i.e., $\Delta p_{inlet} \rightarrow \Delta p_{junction}$), which is one of the dominant parameters in determining slug characteristics. While the characteristics vary from previous experiments, the trends (i.e., longer slugs as air pressure is decreased) remain the same, which indicates that this drop in pressure due to the valves merely acts as an offset to previous experimental results and not a fundamental change in the process.

During operation of the experimental system, it also became clear that proper priming was essential to performance. The setup procedure, which involves operating both valves continuously open, required several minutes of operation to reach the periodic flow regime. Next, the valve controlling the air was closed and the water valve was allowed to cycle several times to clear all air out of the junction. At this point the system was prepared for standard operation. Failure to

properly prime the setup in this fashion would prevent slugs from forming and would require the system to be completely dried out before further testing could be performed. While this is possible in the lab environment, it does indicate a high level of quality control needed for post-manufacturing calibration as the performance of the microthruster will be dependent on this setup procedure.

Finally, one phenomenon that was observed during the experiments was a slight residual flow of the liquid after the valve closing. The first assumption, that the valves were leaking, was disproved after testing. Additional investigation seems to suggest that there may be an issue with the compliance of the tubing in the system. When the valve closes, the contraction of the tubing forces some of the liquid to continue to flow downstream. This post-valve flow would clearly be undesirable as it increases the length of time the thruster would continue to operate after shutdown is initiated, reducing the performance of the fuel injection system. For experimental purposes, future iterations of the apparatus will replace plastic tubing with stainless steel, where possible, to eliminate compliance. A final working prototype of the nanosat would use stainless steel tubing, so there should be no issue with compliance.

5. Conclusions

A fuel delivery system with application to nanosatellite micropropulsion has been proposed, which uses the immiscibility of converging flows of a fuel and an inert gas at a micro-scale cross junction to produce disperse microslugs of fuel. Previous works by McDevitt and Hitt (2011) and McCabe *et al.* (2011) have characterized the performance of the fuel delivery system using the microslug characteristics of a steady-state system. In this work, the effect of transient operation on the performance of the fuel delivery system was characterized using numerical and experimental techniques, and compared to the performance of an equivalent steady-state fuel delivery system.

A series of multiphase simulations were performed to numerically study the impact that valve actuation time and surface tension coefficient had on the performance of the system. The results indicated that slow valves for which the fully open time is small compared to the response time can result in an initial slug that is up to 17% longer than the equivalent steady-state slugs, which can lead to a 12% increase in the minimum impulse bit. For implementation in a MEMS-based microthruster system, this limitation may put a lower bound on the minimum impulse bit that can be achieved. The surface tension coefficient, which has been demonstrated to be a dominant parameter in the slug formation process and may vary during a typical mission due to changes in temperature or fuel contamination, had an effect on performance of up to 3%, but typically less than 1% across the range of inlet conditions.

As a complement to the numerical results, flow visualization experiments were performed. Experimental results demonstrated that the system was able to stop and restart with less than a 1% effect on the slugs formed during operation of a miniature solenoid valve with 20 ms actuation time. The performance of the experimental system was also highly sensitive to proper initial setup, which has ramifications on the development of a prototype thruster.

The results of this study are promising for the intended micropropulsion application, as they indicate that the steady-state slug characteristics can be used to predict impulse delivery to within a few percent error without resorting to full transient considerations for slower valves. As valve technology improves, and valve-actuation cycles get faster, the transient effects may be more significant and require further study.

Acknowledgments

This work was supported by NASA Cooperative Agreement # NNX09AO59 and the Vermont Advanced Computing Center.

References

Bouwmeester, J. and Guo, J. (2010), "Survey of worldwide pico- and nanosatellite missions, distributions and subsystem technology", *Acta Astronautica*, **67**, 854-862.

Cubaud, T. and Ho, C. (2004), "Transport of bubbles in square microchannels", *Phys. Fluid.*, **16**(12), 4575-4585.

Cubaud, T., Tatineni, M., Zhong, X. and Ho, C. (2005), "Bubble dispenser in microfluidic devices", *Phys. Rev. E*, **72**(3), 037302.

Garstecki, P., Fuerstmann, M., Stone, H. and Whitesides, G., (2006), "Formation of droplets and bubbles in a microfluidic T-junction-scaling and mechanism of breakup", *Lab. Chip.*, **6**, 437-446.

Hitt, D., Zakrzwski, C. and Thomas, M. (2001), "MEMS-based satellite micropropulsion via catalyzed hydrogen peroxide decomposition", *J. Smart Mater. Struct.*, **10**, 1163-1175

Janson, S. (2008), *The history of small satellites*, Eds. Helvajian, H. and Janson, S., Small Satellites, Past, Present and Future.

Kujawa, J. and Hitt, D. (2004), "Transient shutoff simulations of a realistic MEMS supersonic nozzle", *Proceedings of the 40th AIAA/ASME/SAE/ASEE Joint Propulsion Conference & Exhibit*, Ft. Lauderdale, July.

Lewis, D., Janson, S. and Cohen, R. (2000), "Digital micro-propulsion project", *Sens. Actuat. A*, **80**, 143-154.

Louisos, W. and Hitt, D. (2011), "Analysis of transient flow in supersonic micronozzles", *J. Spacecraft Rock.*, **48**(2), 303-311.

McCabe, J., Hitt, D. and McDevitt, M. (2012), "A micro-scale monopropellant fuel injection scheme using two-phase slug formation", *J. Propuls. Pow.*, **27**(6) 1295-1302

McDevitt, M. and Hitt, D., (2011), "Numerical study of disperse monopropellant slug formation at a cross junction", *Proceedings of the 41st AIAA Fluid Dynamics Conference*, Honolulu, June.

Osher, S. and Sethian, J. (1988), "Fronts propagating with curvature-dependent speed: algorithms based on Hamilton-Jacobi formulations", *J. Comput. Phys.*, **79**, 1249.

Olsson, E. and Kreiss, G., (2005), "A conservative level set method for two phase flow", *J. Comput. Phys.*, **210**, 225-246.

Qian, D. and Lawal, A. (2006), "Numerical study of gas and liquid slugs for Taylor flow in T-junction microchannel", *Chem. Eng. Sci.*, **61**, 7609-7625.

Thorsen, T., Roberts, R., Arnold, F. and Quake, S. (2001), "Dynamic pattern formation in a vesicle generating microfluidic device", *Phys. Rev. Lett.*, **86**, 4163-4166.

EC